

Letter of Intent to PAC 52

Final-State Interactions Studies in Deuterium at Very High Missing Momenta

C. Yero * †

The Catholic University of America, DC

W. Boeglin†, M. Sargsian

Florida International University, FL

M. Jones†

Thomas Jefferson National Accelerator Facility, VA

April 13, 2025

*Contact: yero@cua.edu

†Spokesperson

Executive Summary

One of the most fundamental problems in nuclear physics is to describe the strong nuclear force between protons and neutrons (nucleons) from first principles using Quantum Chromodynamics (QCD) — the fundamental nuclear theory of strong interactions. Understanding the high-momentum structure of the neutron-proton (np) bound system is highly important for nuclear physics due to the observed dominance of short-range correlations (SRCs) in nuclei at nucleon momenta above $\sim 250 - 300$ MeV/c (Fermi momentum). However, to understand the repulsive part of the NN interaction in $A > 2$ bound systems, one must first understand the simplest ($A = 2$) case without added complications that come with many-body nuclear systems. In addition, a solid understanding of final-state interactions (FSI) and how to suppress them is also required as these interactions distort the reconstruction of the internal relative momenta (\vec{p}_i) of the detected nucleon causing any information about the internal structure of the nucleus to be misinterpreted.

The first high momentum transferred ($Q^2 > 1$ (GeV/c) 2) studies on the deuteron carried out at Jefferson Lab during the 6-GeV era showed a strong angular dependence of FSI with respect to the neutron recoil angle relative to the momentum transferred (θ_{nq}) where FSI were found to be the strongest at $\theta_{nq} \sim 70^\circ$, while being significantly reduced at forward angles, $\theta_{nq} \sim 30 - 40^\circ$ for neutron recoil (“missing”) momenta up to $p_m \sim 550$ MeV/c. However, no data that studies this angular dependence currently exists above $p_m \sim 550$ MeV/c, a kinematic region where the nucleons are expected to significantly overlap and a transition from nucleonic to quark-gluon description of the nucleus is predicted to occur. Therefore, it becomes crucial to have a solid understanding of FSI at very high missing momenta.

We propose to measure the exclusive unpolarized electro-disintegration of the deuteron in Hall C with a 10.55-GeV electron beam incident on a 10-cm long liquid deuterium target. The scattered electrons will be detected by the Super High Momentum Spectrometer (SHMS) in coincidence with the knocked-out protons detected by the High Momentum Spectrometer (HMS), and the recoil (“missing”) neutrons will be reconstructed from momentum conservation. We will focus on the high missing momentum region of $p_m = 800$ MeV/c and measure the unpolarized absolute cross sections for three central recoil angles: $\theta_{nq} = 49^\circ, 60^\circ, 72^\circ$ at $Q^2 = 4.5$ (GeV/c) 2 . To extract the angular distributions, a ratio of data cross-sections to a theoretical model of the plane-wave impulse approximation (PWIA) will be taken for a range of recoil angles. This will allow us to precisely determine at which recoil angles FSI are large (or small). To compare the data to theory angular distributions, the ratio of FSI/PWIA will also be taken for different deuteron theoretical calculations using either the CD-Bonn, AV18 or Paris NN potentials.

We request a total of 548 hrs (23 PAC days) which consists of 540 hrs of physics production and 8 hrs reserved for overhead. This work will complement and contribute to the recent ongoing efforts to explore the elusive deuteron repulsive core, a topic of high theoretical interest motivated by the discrepancy between theory and our recent experimental results of the deuteron electro-disintegration at missing momenta where a transition from nucleonic to quark-gluon description of matter is expected to occur.

Contents

1 Motivation	4
2 Experimental Program	8
3 Proposed measurement	10
3.1 Experimental Method	10
3.2 Simulations	11
3.2.1 Kinematics	13
3.2.2 Acceptance	16
3.3 Projected results	17
3.4 Systematic Uncertainties	20
4 Run Plan	21
5 Summary	22

1 Motivation

The deuteron is the most simple bound structure in nuclear physics and is therefore the “ideal laboratory” to study the nuclear short-range interaction. More specifically, when protons and neutrons come in close proximity, at extremely short distances ($\sim 10^{-15}$ m), they must experience a very strong repulsive force that keeps normal matter from collapsing. Unfortunately, not much progress has been made with respect to this aspect of the nuclear force from both a theoretical and experimental standpoint. From the experimental aspect, the limitations have been mainly the low incident electron energies used to probe the nucleus as well as the spectrometer capabilities to detect such high energies. From the theoretical standpoint, since the construction of most nucleon-nucleon (NN) interaction models rely in part in experimental NN scattering data used to constrain the models, a significant advancement in the understanding of the nuclear core has been restricted.

The most direct way to probe the repulsive core of the deuteron np bound-state is via the exclusive $d(e, e'p)$ reaction (see Fig.4). Since the deuteron is a two-body system, we can identify its final state precisely (hence, *exclusive*) and select kinematics to emphasize quasi-elastic knockout of the proton (referred to as plane-wave impulse approximation or PWIA) without competing processes such as (i) neutron-proton re-scattering effects also referred to as final-state interactions (FSI), (ii) meson-exchange currents (MEC) where the virtual photon couples to the exchanged meson or (iii) nuclear excitation into a resonance state (isobar currents or IC), each of which would distort the relationship between the neutron recoil (“missing”) momentum, p_m , and the proton initial momentum, p_i . The relative internal momentum of the bound proton can then be inferred from the reconstructed p_m .

Previous deuteron electro-disintegration experiments carried out at $Q^2 < 1$ (GeV/c) 2 (see Sec.5 of Ref. [1]) have helped quantify the contributions from FSI, MEC and IC to the $d(e, e'p)$ cross sections and determine kinematics at which these processes are either suppressed (MECs and ICs) or under control (FSI). At larger Q^2 , MEC and IC are expected to be suppressed at $Q^2 > 1$ (GeV/c) 2 , and by selecting Bjorken $x_{Bj} \equiv Q^2/2M_p\nu > 1$ (M_p is the proton mass and ν is the energy transferred) where the lower energy transferred (ν) part of the quasielastic peak is maximally away from the inelastic resonance production threshold. Even at $Q^2 > 1$ (GeV/c) 2 and $p_m \gtrsim 300$ MeV/c however, FSI are still the dominant contribution to the cross sections compared to the PWIA, therefore they must be studied more carefully.

Final-state interactions have been studied theoretically by several groups [2–9]. In particular, one of the most important results of these studies is described by the generalized eikonal approximation (GEA) initially developed in Refs. [3, 4]. The establishment of the eikonal regime at $Q^2 > 1$ (GeV/c) 2 is characterized by a very anisotropic angular distribution of the neutron recoil angles relative to the 3-momentum transfers, θ_{nq} , and it makes it possible to identify kinematics where FSI are mostly cancelled (see Fig.1).

The GEA predicts a FSI peak at $\theta_{nq} \sim 70^\circ$ for $p_m \sim 500$ MeV/c. This prediction was confirmed by the first set of high- Q^2 deuteron electro-disintegration experiments carried out at Jefferson Lab [10, 11] (see Fig. 2). Additionally, it was also found that at very forward and backward neutron recoil angles of $\theta_{nq} \sim 40^\circ, 120^\circ$ FSI were significantly reduced and comparable to the PWIA.

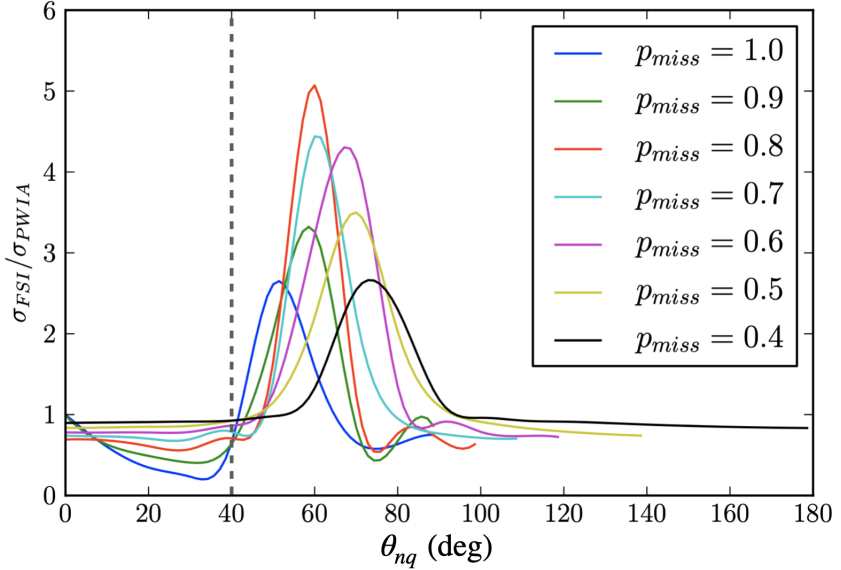


Figure 1: Ratios of the calculated FSI to PWIA cross sections (using the CD-Bonn potential) for different missing momenta as a function of the neutron recoil angle. Note: Reprinted from Ref. [1].

The reduction in FSI can be understood from the fact in the high energy limit ($Q^2 > 1$ (GeV/c) 2) of the GEA, the np re-scattering amplitude is mostly imaginary:

$$A = A_{\text{PWIA}} + iA_{\text{FSI}}, \quad (1)$$

with $A_{\text{FSI}} \approx i|A_{\text{FSI}}|$, where the total scattering amplitude A is expressed as the sum of the PWIA (A_{PWIA}) and the imaginary part of the FSI (A_{FSI}) scattering amplitudes. The total theoretical cross section can then be obtained by taking the modulus square of the total scattering amplitude and can be expressed as

$$\sigma_{\text{FSI}} \sim |A|^2 = |A_{\text{PWIA}}|^2 - 2\underbrace{|A_{\text{PWIA}}||A_{\text{FSI}}|}_{\text{"Screening" or interference term}} + \underbrace{|A_{\text{FSI}}|^2}_{\text{re-scattering term}}. \quad (2)$$

Taking the ratio of the total to the PWIA part of the cross section,

$$R = \frac{\sigma_{\text{FSI}}}{\sigma_{\text{PWIA}}} = 1 - 2\frac{|A_{\text{PWIA}}||A_{\text{FSI}}|}{|A_{\text{PWIA}}|^2} + \frac{|A_{\text{FSI}}|^2}{|A_{\text{PWIA}}|^2}. \quad (3)$$

From the ratio of cross sections the interference term enters with an opposite sign as compared to the re-scattering term, which provides an opportunity for an approximate cancellation at certain neutron recoil angles as shown in Figs. 1 and 2. This cancellation is also approximately independent of the neutron recoil momenta, which opens a kinematic window at $\theta_{nq} \sim 40^\circ$ where one can probe the short-range structure of the deuteron beyond $p_m \sim 500$ MeV/c.

Another important feature of the GEA, and perhaps the one most relevant to this letter is that the FSI peak, originally at $\theta_{nq} \sim 70^\circ$ for $p_m = 0.5$ GeV/c, shifts toward smaller

recoil angles with increasing missing momenta as shown in Fig.1. This raises a very important question regarding the experimental sensitivity of the high-momentum component of the deuteron to FSI. In the most recent deuteron electro-disintegration experiment at Hall C [12], the internal momentum probed was extended up to $p_m \sim 940$ MeV/c (see Fig.3) at kinematics optimized for reducing FSI, based on the results from Ref. [10] (see Fig.2), by selecting central recoil angles $\theta_{nq} \sim 40^\circ$.

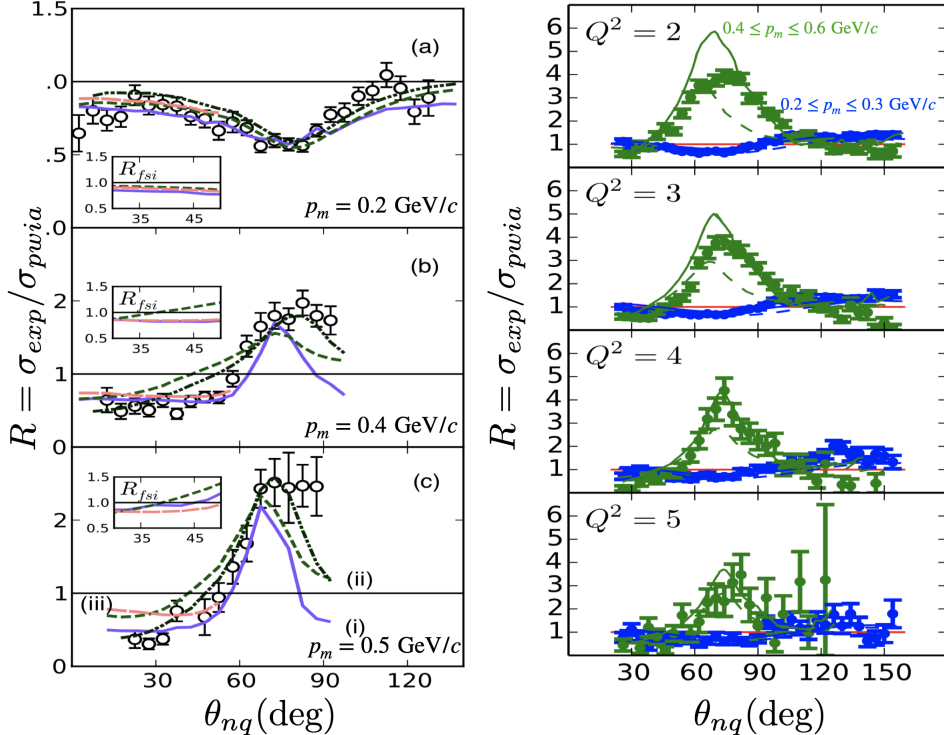


Figure 2: ${}^2\text{H}(e, e'p)n$ angular distributions of the cross section ratio, $R = \sigma_{exp}/\sigma_{pwia}$. (Left) Hall A data at $Q^2 = 3.5 \pm 0.25$ (GeV/c) 2 and missing momentum settings (a) $p_m = 0.2$ GeV/c, (b) $p_m = 0.4$ GeV/c and (c) $p_m = 0.5$ GeV/c. Theoretical calculations for (i) solid (purple) curves using the CD-Bonn potential by M. Sargsian [8], (ii) dashed (green) curves using FSI and dashed-double dotted (black) curves using FSI+MEC+IC by J.M. Laget [6] using the Paris potential and (iii) dashed (pink) curves denote calculations by J.W. Van Orden [7]. (Right) Hall B data at various Q^2 settings. The green data (with FSI re-scattering peak) correspond to $400 \leq p_m \leq 600$ MeV/c, and the blue data (no FSI re-scattering) correspond to $200 \leq p_m \leq 300$ MeV/c. The solid curves are calculations from J.M. Laget [6] and the dashed curves are from M. Sargsian [8]. Note: Reprinted from Ref. [1].

As shown in Fig.3, the data agrees well with the previous Hall A measurements [10] and is reproduced by all deuteron calculations for missing momenta up to $p_m \sim 550$ MeV/c, however, no theoretical model reproduces the data for $p_m \geq 750$ MeV/c. This disagreement can be attributed to an enhanced role of the relativistic effects as well as a possible indication of the onset of non-nucleonic degrees of freedom given that $p_m \sim 750$ MeV/c corresponds to the inelastic threshold in the np channel [13].

Furthermore, from Fig.3 it is interesting to note that the onset of FSI (solid magenta for CD-Bonn calculations) starts already at $p_m \sim 800$ MeV/c for $\theta_{nq} = 35 \pm 5^\circ$, and as early as $p_m \sim 600$ MeV/c for $\theta_{nq} = 45 \pm 5^\circ$.

It is also important to emphasize that the current theoretical calculations of the deuteron model including FSI do not yet account for relativistic effects. The theoretical calculations to include relativistic effects including FSI in the light-front reference frame are currently being developed by M. Sargsian.

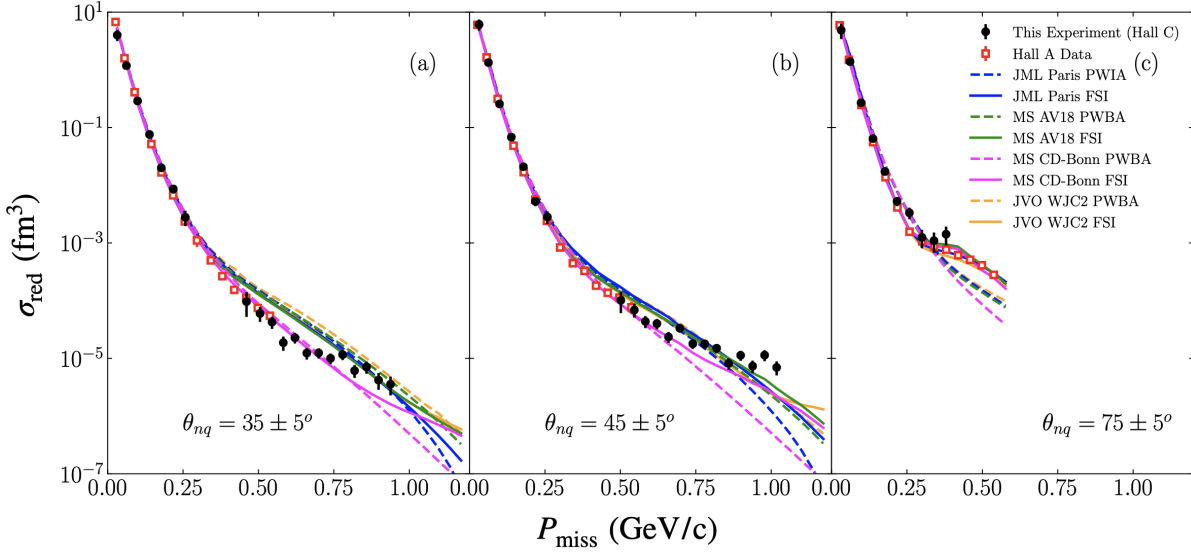


Figure 3: The experimental reduced cross sections (momentum distributions) for three values of the recoil angle θ_{nq} at $Q^2 = 4.5 \pm 0.5$ (GeV/c) 2 [12]. The solid lines are calculations including FSI and the dashed lines correspond to PWIA calculations [8].

In this letter of intent, we therefore propose to extend the angular distributions measured in Ref. [10] (see Fig.2 (left)) to a central missing momentum of $p_m = 800$ MeV/c, a critical region corresponding to the repulsive core around which none of the deuteron models is able to reproduce the data in Fig.3. These proposed measurements will enable us to determine more precisely, the kinematic regions where FSI are reduced, as well as separate the effects of FSI from possible contributions of non-nucleonic components of the deuteron [13], which are expected to show up around $p_m \sim 800$ MeV/c. In addition, we can also explore the possibility of carrying out a similar measurement for the next complicated nucleus, Helium-3, to map out the angular dependence of FSI with a 3-body system. There exist calculations by Sargsian *et al.* [14] which investigate the various features of the ${}^3\text{He}$ electro-disintegration which include FSI calculations, however, no experimental measurement of the FSI angular dependence with θ_{rq} exists for this nucleus. These measurements will provide an experimental ground to precisely select regions of small FSI that will enable to probe more precisely the momentum distributions of both the deuteron and Helium-3.

2 Experimental Program

We propose to measure the $d(e, e'p)n$ absolute cross sections at $Q^2 = 4.5 \pm 0.5$ (GeV/c) 2 for 3 central recoil angles: $\theta_{nq} = 49^\circ, 60^\circ, 72^\circ$ corresponding to a central missing momentum setting of $p_m = 800$ MeV/ c . The selected recoil angles will provide a wide angular coverage to map out the FSI dependence on θ_{nq} . The angular distributions will be extracted by taking the ratio of the experimental cross sections to the PWIA theoretical cross sections versus neutron recoil angles, θ_{rq} . At such high Q^2 , it is expected that MEC and IC will have negligible contributions to the experimental cross sections for forward recoil angles. At larger angles ($\theta_{nq} > 70^\circ$), where $x_{Bj} < 1$, however, IC can still contribute significantly due to being near the inelastic electroproduction threshold, as evidenced by the data points in the last panel in Fig.2(left).

Measurements will also be done at $p_m = 500$ MeV/ c for $\theta_{nq} = 70^\circ$ at the same Q^2 . These data will be used for normalization measurements and comparison to the Hall A data [10]. In addition, we will also measure the ${}^1\text{H}(e, e'p)$ hydrogen elastic reaction to (i) check the spectrometer acceptance models, (ii) study target boiling effects and (iii) check systematic effects on beam energy and the spectrometer's central momentum and angle.

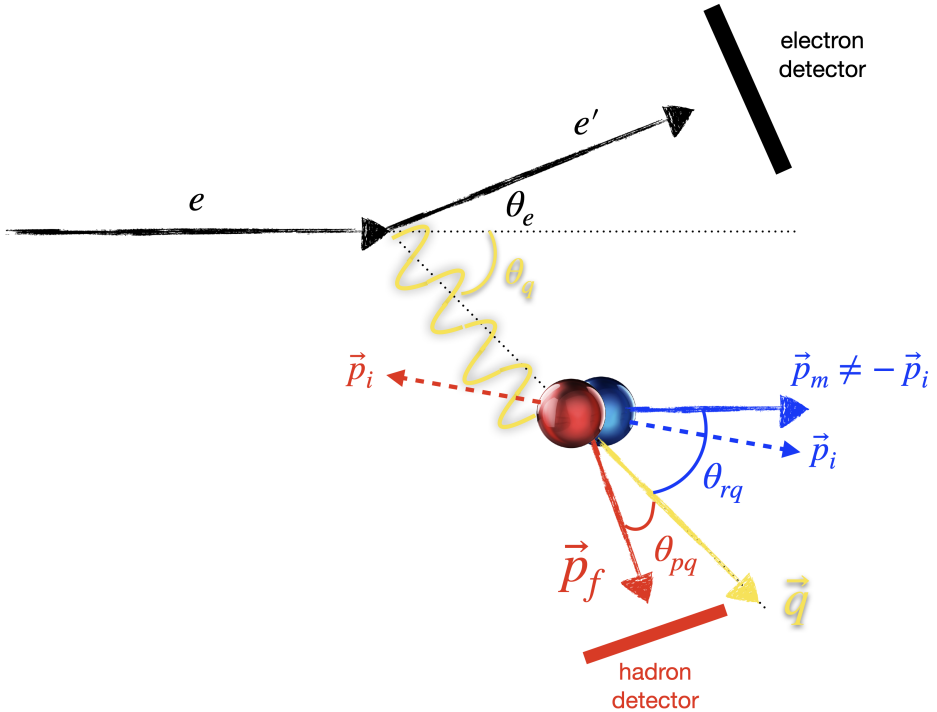


Figure 4: Schematic diagram of the $d(e, e'p)n$ reaction.

The experiment will be carried out at Jefferson Lab Experimental Hall C. A 10.55-GeV, 3x3 mm 2 square-rastered electron beam will be incident on a 10-cm long liquid deuterium target. A typical $d(e, e'p)n$ reaction is shown in Fig.4 in which the incident electron interacts with the deuteron via the one-photon exchange approximation (OPEA), in which the scattered electron (k_f, θ_e) is detected by the Super High Momentum Spectrometer (SHMS) in coincidence with the knocked-out proton (p_f, θ_p) detected by the High Momentum Spectrometer

(HMS). The recoil neutron momenta (\vec{p}_m) is reconstructed from momentum conservation. In Fig.4, the dashed vectors represent the relative internal momenta of the bound nucleons before interacting with the virtual photon. After the interaction, the bound proton is directly knocked-out, modifying its momentum. Within the PWIA, the spectator neutron would recoil with a missing momentum $\vec{p}_m = -\vec{p}_i$. However, due to FSI, the neutron re-interacts with the proton causing a modification in its recoil momentum such that $\vec{p}_m \neq -\vec{p}_i$. The modification of the neutron recoil momentum by FSI destroys any information related to the internal momentum of the deuteron. In either case, the modified missing momentum is determined by the vector difference $\vec{p}_m = \vec{q} - \vec{p}_f$, as shown in Fig.5. The central spectrometer kinematics are summarized in Table 1. A detailed description of the kinematics is covered in Section 3.2.1.

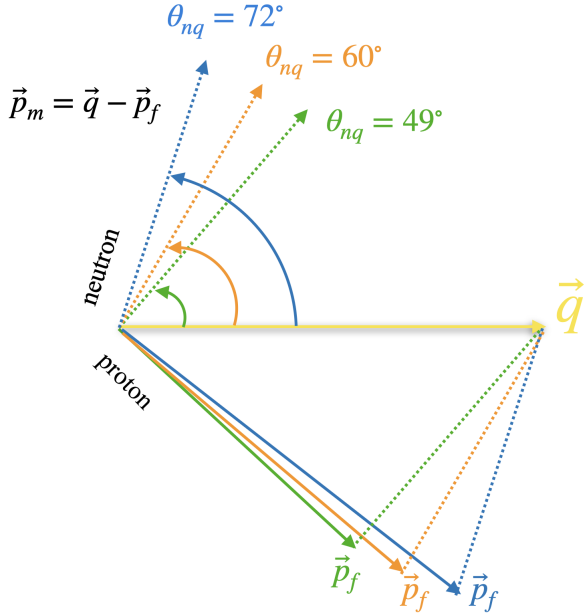


Figure 5: Schematic diagram showing the vector reconstruction of the recoil neutron \vec{p}_m from the virtual photon momentum transferred, \vec{q} , detected proton, p_f for each of the three central recoil angles, θ_{nq} . The dashed lines at the proton side are for reference.

p_m (MeV/c)	θ_{nq} (deg)	k_f (GeV/c)	θ_e (deg)	p_f (GeV/c)	θ_p (deg)
500	70	8.151	13.14	3.069	44.17
800	49	8.551	12.82	2.468	54.85
	60	8.151	13.14	2.891	49.27
	72	7.552	13.65	3.516	41.57

Table 1: Central spectrometer kinematics coverage for an incident electron beam energy of $E_b = 10.55$ GeV and $Q^2=4.5$ $(\text{GeV}/c)^2$.

3 Proposed measurement

In the following section we describe the experimental observable, the expected kinematic coverage from simulations and the expected results.

3.1 Experimental Method

Assuming the PWIA in which the virtual photon couples directly to the bound proton, which is subsequently ejected from the deuteron without any further interaction with the recoiling neutron, the neutron carries a momentum equal in magnitude but opposite in direction to the initial momentum of the bound proton, $\vec{p}_m = -\vec{p}_i$, thus providing information on the momentum of the bound proton and its momentum distribution. However, if FSI are accounted for, the neutron momentum is modified by re-scattering with the knocked-out proton, and $\vec{p}_m \neq -\vec{p}_i$. For this specific case, assuming IC and MEC are negligible, one can still factorize the differential cross-section as follows:

$$\frac{d^6\sigma}{dE'd\Omega_e d\Omega_p dT_p} = K \cdot \sigma_{eN} \cdot S_D(\vec{p}_m \neq \vec{p}_i, E_m), \quad (4)$$

where K is a kinematic factor and σ_{eN} describes the elementary cross section for an electron scattering off a bound (off-shell) nucleon where the deForest [15] off-shell cross sections, σ_{cc1} or σ_{cc2} , are commonly used. The $S_D(\vec{p}_m, E_m)$ is referred to as a “distorted” spectral function, due to the modification of the recoil neutron momentum. In the approximation of $p_m \sim p_i$ (PWIA), the spectral function $S(\vec{p}_m \approx \vec{p}_i, E_m)$ would otherwise describes the probability of finding a bound proton with momentum \vec{p}_i and separation (“missing”) energy E_m .

We use the standard definition of missing energy: $E_{\text{miss}} = \nu - T_p - T_{\text{rec}}$, where ν is the energy transferred to the nucleus, and (T_p, T_{rec}) are the proton and recoil kinetic energies, respectively. For the special case of a deuteron break-up reaction, the recoil kinetic energy refers to that of the neutron. Since the deuteron has no excited states, the kinetic energies of the proton and neutron are well-defined and the missing energy becomes the binding energy of the deuteron, ~ 2.2 MeV. It follows that for the special case of the deuteron bound state, the separation (binding) energy can be integrated out of Eq. 4 to obtain,

$$\sigma_{\text{theory}} \equiv \frac{d^5\sigma_{\text{theory}}}{dE'd\Omega_e d\Omega_p} = K f_{\text{rec}} \sigma_{eN} S_D(\vec{p}_m), \quad (5)$$

where f_{rec} is the recoil factor that arises from the integration in E_m and is defined as [16]

$$f_{\text{rec}} \equiv \frac{1}{1 - \frac{1}{2} \frac{E_f q^2 - (p_f^2 + p_m^2)}{E_r p_f^2}}. \quad (6)$$

where E_f is the final proton energy and E_r is the final neutron recoil energy (note this is different than E_m). From the experimental side, one can then take the ratio of the experimental cross sections to the theoretical cross sections only within the PWIA and bin the events in θ_{nq} to extract the angular distributions, similarly to the ones shown in Fig.2.

3.2 Simulations

The standard Hall C $A(e, e'p)$ coincidence simulation package (SIMC) was used to estimate the count rates for electron-scattering off a 10-cm long liquid deuterium target. The $d(e, e'p)n$ reaction was simulated for each of the central kinematics described in Table 1. The events were weighted by the theoretical model of the deuteron from J.M. Laget for both PWIA and FSI (Paris NN potential) [6]. Furthermore, an efficiency factor based on the prior deuteron experiment [12] was also applied to the weight in order to account for experimental detector tracking inefficiencies in HMS/SMS (3% / 4%), data-acquisition dead-time (1%), target boiling effects (5%) and proton absorption (5%), which further reduced the yield in order to have a more conservative estimate.

additional simulation effects:

To have a more realistic estimate of the count rates, (i) *radiative* and (ii) *energy loss* effects were also included in the simulation. Radiative effects can significantly change the electron kinematics and therefore the measured yields. Energy loss effects account for the particles passage through the detector/spectrometer entrance and exit windows which also leads to a measurable effect in the yields.

event-selection cuts:

To select $d(e, e'p)$ coincidence events, we used the standard definition of missing energy in: $E_{\text{miss}} = \nu - T_p - T_{\text{rec}}$ previously defined in Section 3.1. Due to the finite energy resolution of the spectrometers, however, the binding energy of the deuteron is spread about its central value. In addition, spectrometer momentum ($\Delta P/P_0$) and angular acceptance cuts were also applied. The momentum acceptance refers to a relative variation of the detected particle momentum, ΔP , with respect to the spectrometer central momentum, P_0 . The angular acceptance refers to a relative variation in the scattered particles in-plane and out-of-plane angles with respect to the central spectrometer angle. The events are reconstructed and projected back to a collimator where the angular acceptance cut is applied. A summary of the cuts applied is presented in Table 2. The kinematics distributions are shown in 3.2.1.

analysis cut	range
E_{miss}	-20 to 40 MeV
Q^2	4 to 5 $(\text{GeV}/c)^2$
HMS $\Delta P/P_0$	-10 to 10 %
SHMS $\Delta P/P_0$	-10 to 22 %
HMS collimator	octagonal
SHMS collimator	octagonal

Table 2: SIMC event-selection cuts

background contributions:

From the previous $d(e, e'p)n$ coincidence experiment at Hall C [12], it was shown that the background sources were negligible as shown in Fig.6 (left) where the electron singles (SHMS), proton (HMS) singles and coincidence rates. The right panel of that same figure shows a typical coincidence time spectrum for the $p_m = 80 \text{ MeV}/c$ setting. Therefore, we expect that the background contributions and trigger rates will not be a problem for the proposed experiment, where the only difference are the neutron recoil angles explored.

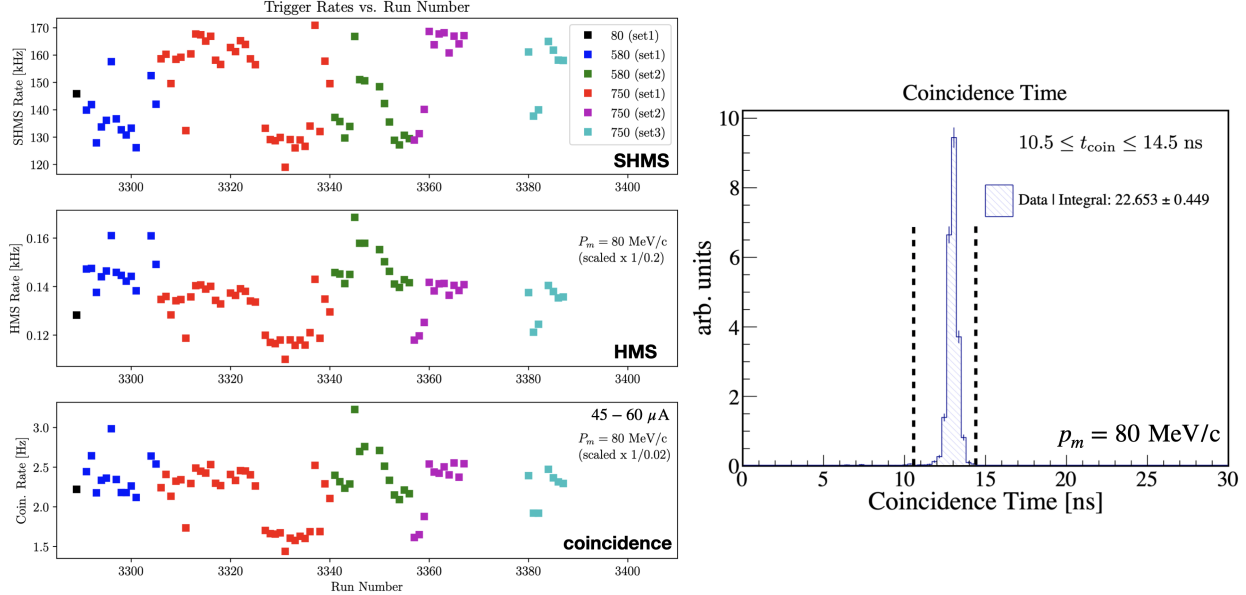


Figure 6: Trigger rates for the SHMS (top, in kHz), HMS (middle, in kHz) and coincidence trigger (bottom, in Hz) during the E12-10-003 experiment. Reprinted from Ref. [17].

count rate estimates:

p_m (MeV/c)	θ_{nq} (deg)	$d(e, e'p)$ rates (counts/hr)	DAQ rates (Hz)	beam-on-target (hrs)
500	70	456	0.467	12
800	49	41	0.0585	200
	60	105	0.101	144
	72	114	0.105	160

Table 3: $d(e, e'p)n$ rate estimates using the Laget FSI model with incident beam energy of 10.55 GeV at $80 \mu\text{A}$. Data-Acquisition (DAQ) rates exclude analysis cuts.

The following subsections show the relevant kinematic and acceptance variables with all event-selection cuts (Table2) and appropriately scaled by the beam-on-target.

3.2.1 Kinematics

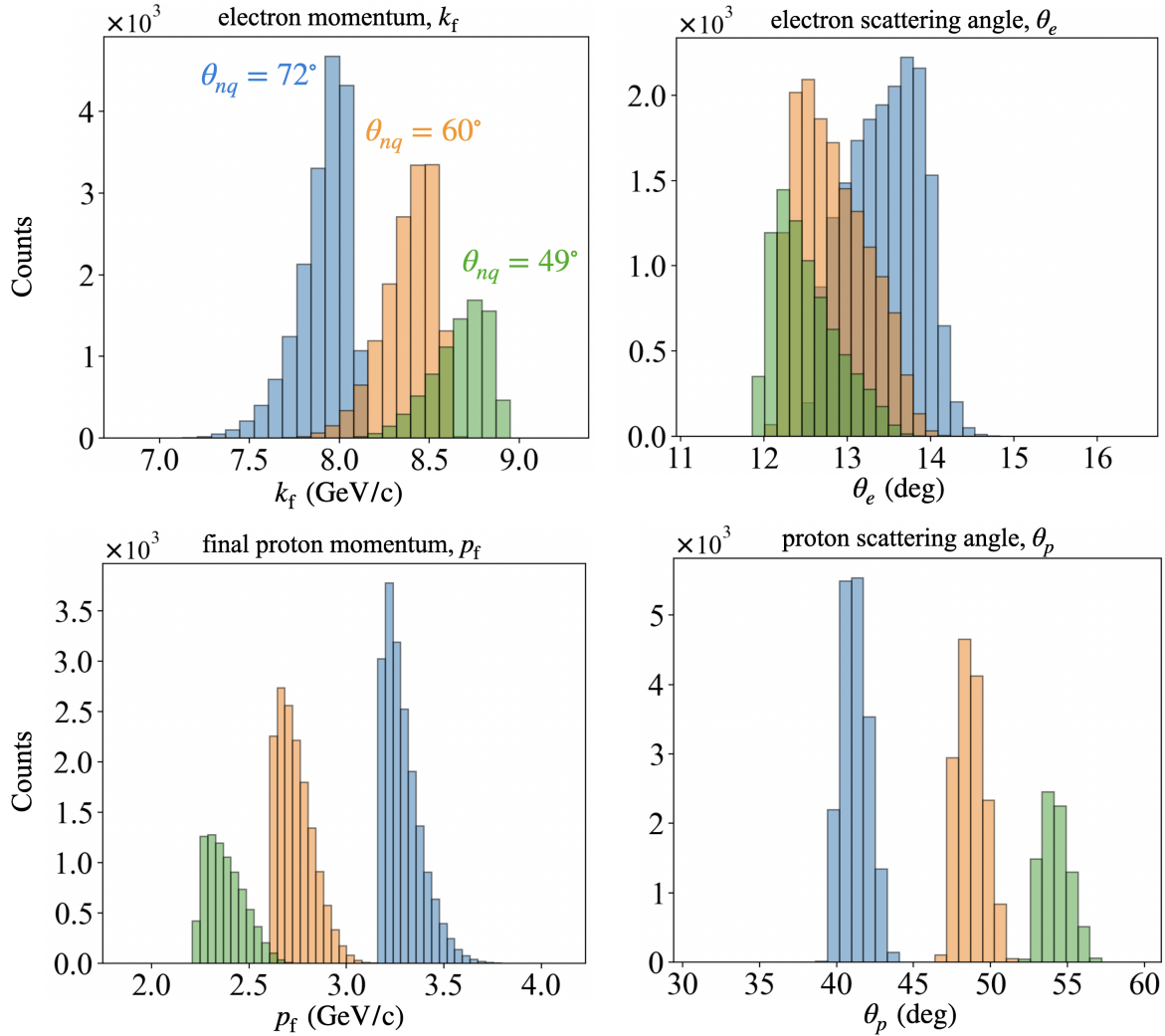


Figure 7: Simulated spectrometer kinematic distributions for SHMS (electrons) and HMS (protons) at 80 μA .

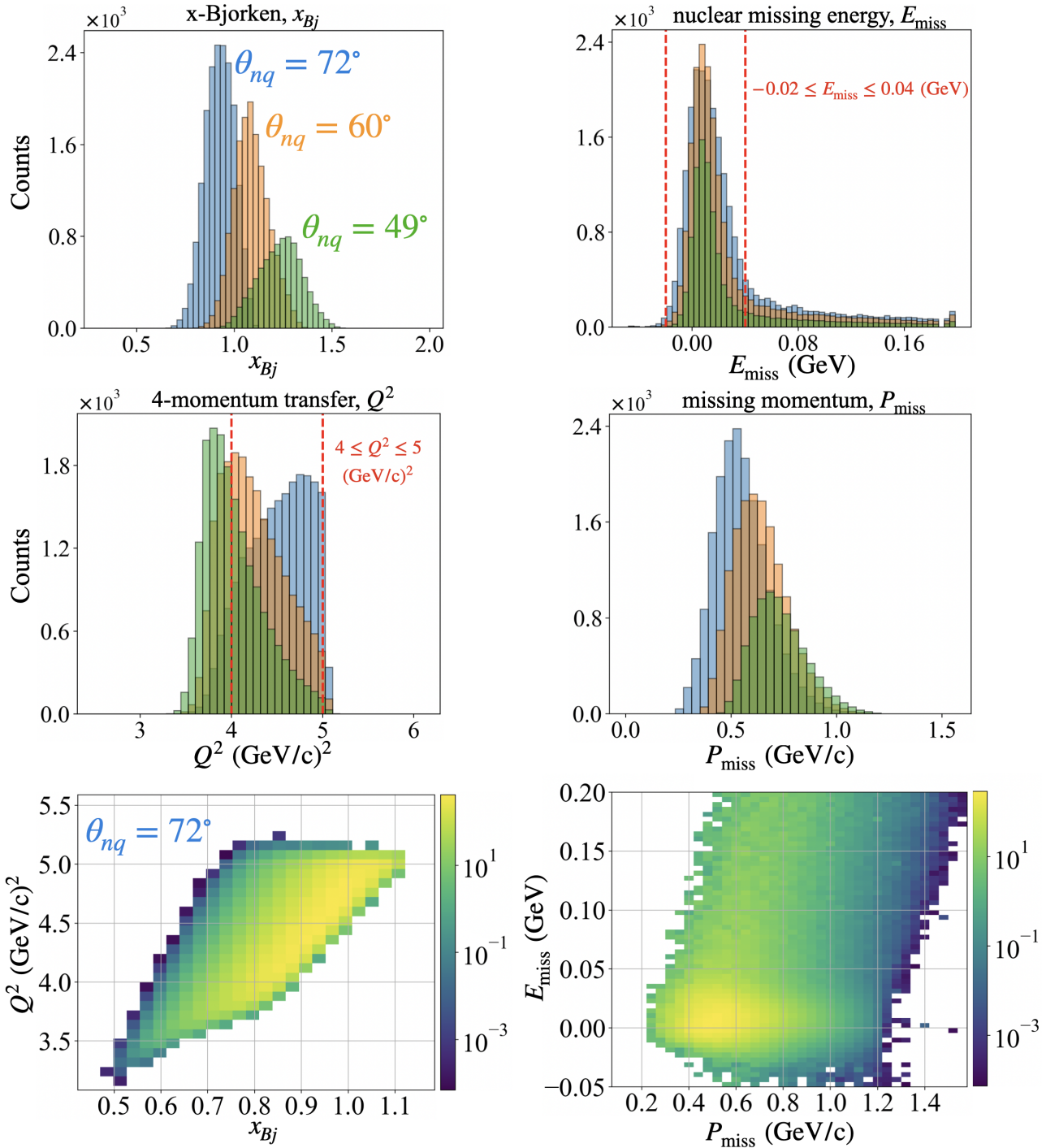


Figure 8: Additional kinematic distributions for x_{Bj} and Q^2 : (bottom 2 panels) 2D correlations of Q^2 vs. x_{Bj} (left) and E_{miss} vs. P_{miss} only for $\theta_{nq} = 72^\circ$. The color bar indicates the counts.

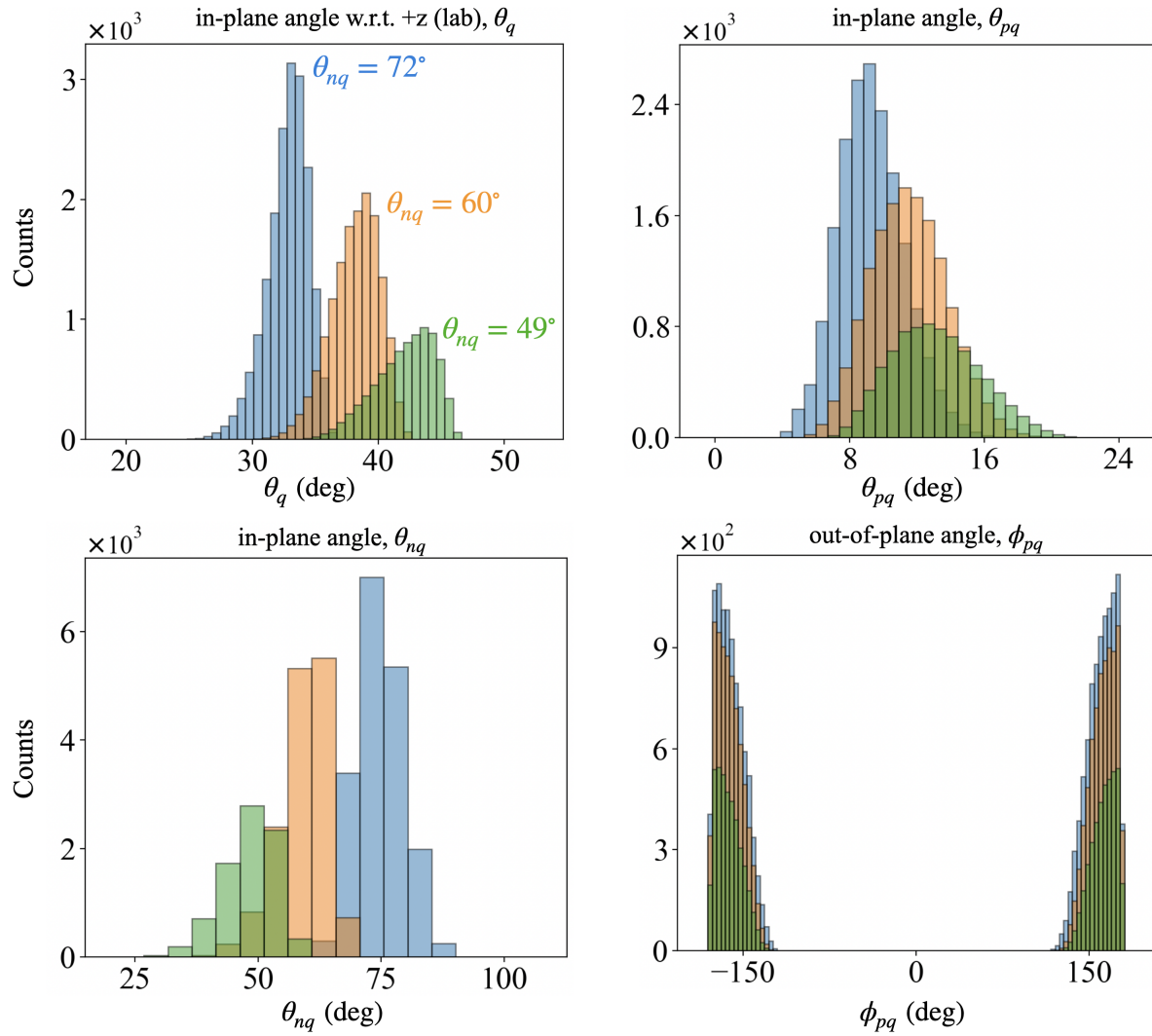


Figure 9: Angular kinematics showing the angles of \vec{q} and the angles of the proton and neutron relative to \vec{q} at $80 \mu\text{A}$.

3.2.2 Acceptance

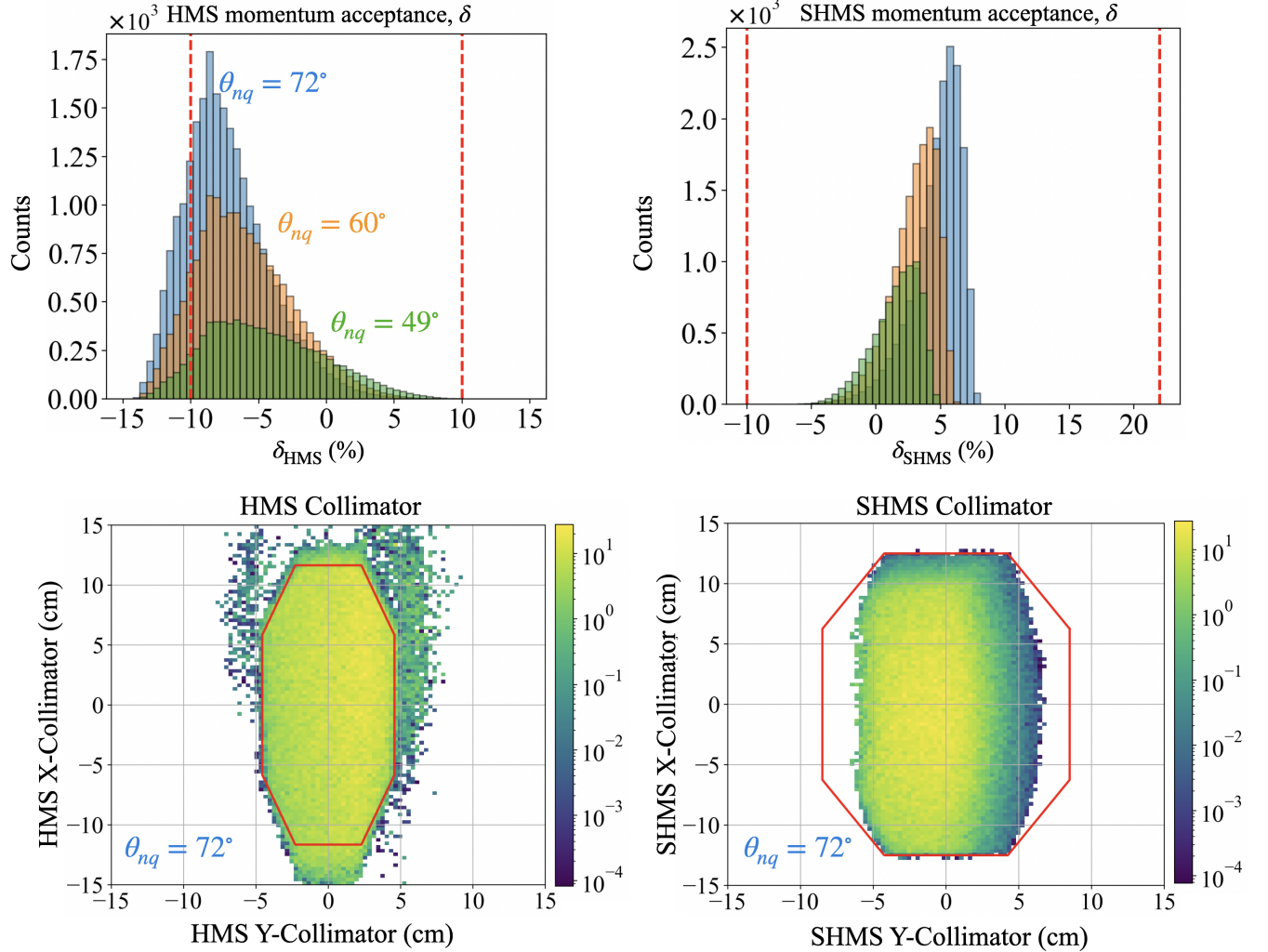


Figure 10: Momentum (top) and angular (bottom) acceptance distributions. The bottom panels show a contour line indicating the collimator geometry boundary; the HMS collimator determine the acceptance of the SHMS, as evidenced by most events in SHMS acceptance falling within the collimator geometry.

3.3 Projected results

The simulation yield for both PWIA and FSI are binned in terms of $(p_{\text{miss}}, \theta_{nq})$ as shown Fig.11(top:FSI, bottom: PWIA). All analysis cuts summarized in Table2 have been applied.

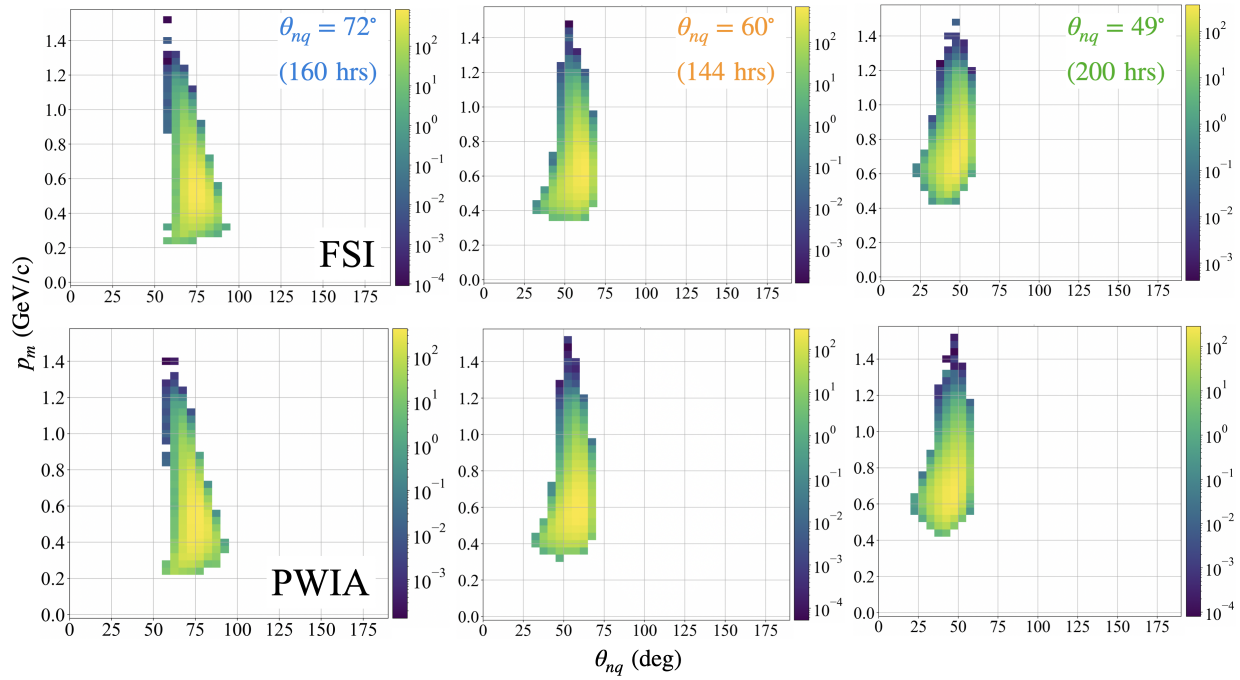


Figure 11: 2D correlation yield of p_{miss} vs. θ_{nq} for $\theta = 49, 60, 72^\circ$ using Laget FSI model [6].

To extract the angular distributions, the ratios of the 2D FSI to PWIA were taken for each (p_m, θ_{nq}) bin presented in Fig.11. The resulting ratio was then plotted versus θ_{nq} for different slices of p_m as shown in Fig.12. From the angular distributions, a FSI peak is clearly visible and starting at $\theta_{nq} = 70^\circ$ in the first p_m bin, and shows a gradual shift towards forward angles. One can also observe that the crossing at $\theta_{nq} \sim 40^\circ$, where the ratio is 1, is consistent throughout all the bins indicating the kinematic region where cancellation between the FSI and the PWIA/FSI interference term occurs, as was discussed earlier. Theoretical calculations that include relativistic effects for high p_m are currently being developed by M. Sargsian using both the CD-Bonn and the AV18 potentials.

Figure 13 shows the projected statistical relative error on the FSI/PWIA ratios from Fig.12, where the red (dashed) lines used as a reference, represent the $\pm 20\%$ relative error mark, showing that most of the data points fall well within a statistical uncertainty of 20%. The beam-on-target time corresponding to the combined three central θ_{nq} settings (the bulk of the experiment) is 504 hrs (21 PAC days).

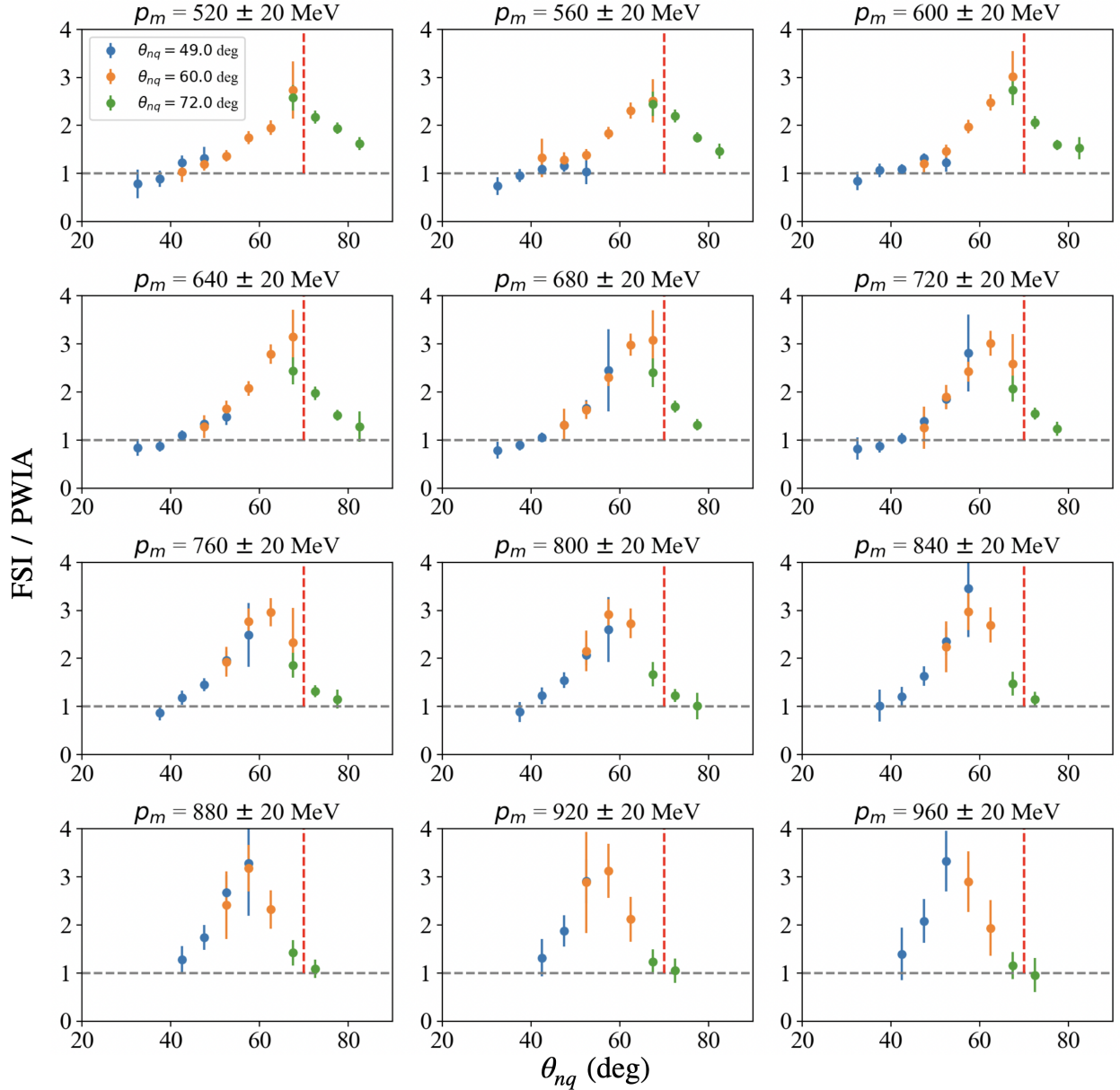


Figure 12: Angular distributions for θ_{nq} for $\theta = 49, 60, 72^\circ$ for a range of p_m bins using the Laget model of the deuteron. The dashed (gray) line at 1 is used as a reference indicating no FSI. The dashed red line is placed at $\theta_{nq} = 70^\circ$ for reference, to more easily observe the shift in the FSI peak.

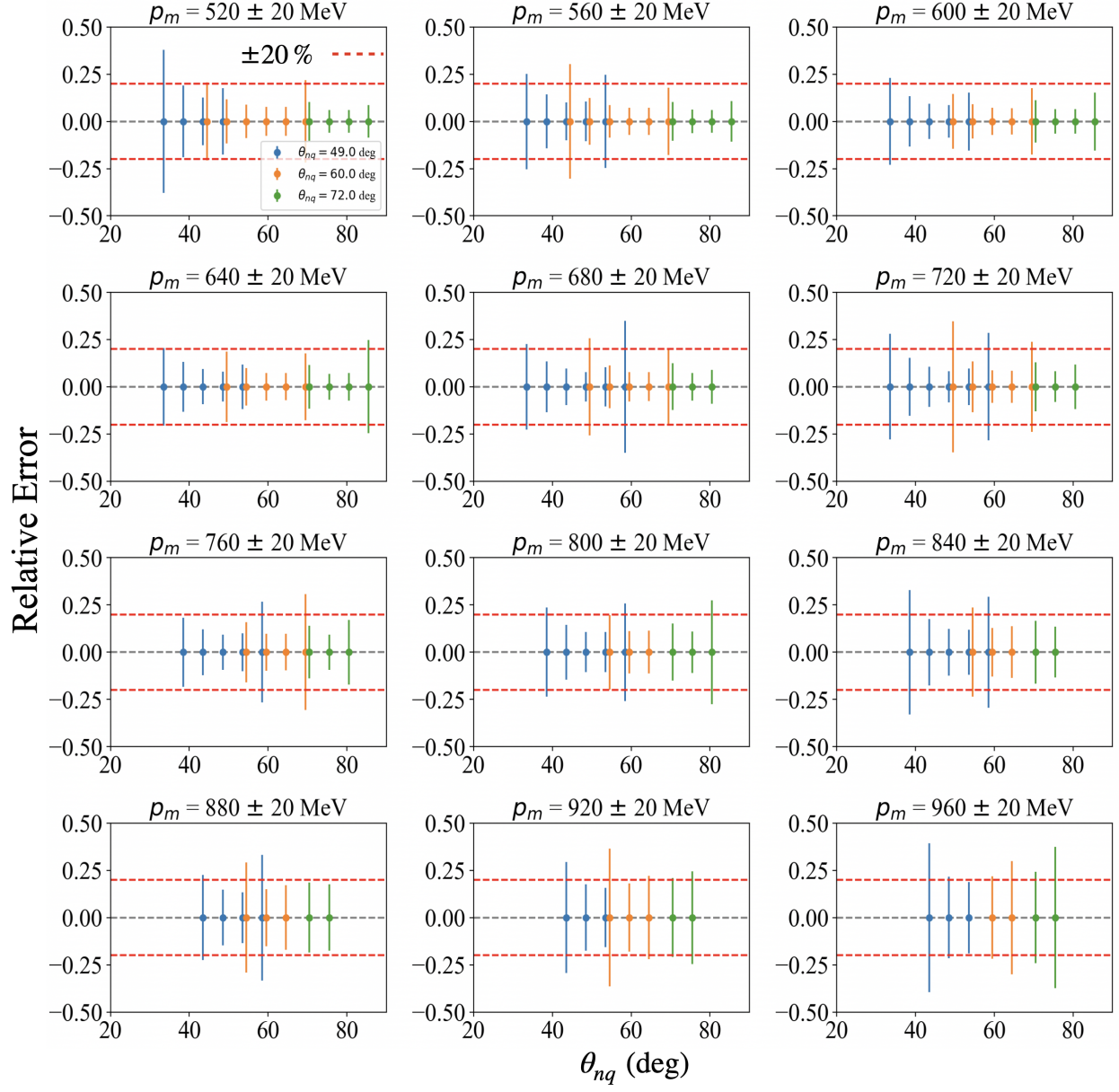


Figure 13: Relative error of angular distributions for θ_{nq} for $\theta = 49, 60, 72^\circ$ for a range of p_m bins using the Laget model of the deuteron. The dashed red lines indicate a $\pm 20\%$ relative error used as a reference.

3.4 Systematic Uncertainties

From the previous $d(e, e'p)$ measurements at Hall C [12, 17], which covered the range of missing momentum as that presented in this letter, the major source of systematic uncertainties were well below 10%. There are two major sources of systematic uncertainties: (i) normalization, and (ii) kinematics.

The normalization uncertainties were typically on the order of 3 – 4% mainly due to the beam-current monitoring (BCM) calibration used in determining the charge normalization factor, the data acquisition dead time corrections as well as target boiling and proton absorption normalization corrections, as described in Ref. [17].

The kinematics uncertainties come mainly from the uncertainty in the determination of the incident beam energy as well as the spectrometers’ momentum and angle settings. These are usually determined by a series of dedicated hydrogen elastic data. From Ref. [12], these uncertainties were determined point-to-point in (p_m, θ_{nq}) bin and were added in quadrature for overlapping bins, with an overall kinematic uncertainty below 6.5%.

Given the similarity between the proposed experiment in this letter and the commissioning deuteron experiment [12], we are confident that the overall systematic uncertainties will not go above 10%.

4 Run Plan

We propose a total of 548 hrs (~ 23 PAC days) with 10.55-GeV beam energy, which consists of 540 hrs of physics production and 8 hrs of overhead. The overhead will be primarily allocated for the spectrometer momentum/angle changes between each of the central settings. Table gives an overview of the time allocations for each part of the experiment.

From past experience on the data analysis of $d(e, e'p)$ at high missing momentum in Hall C [12, 17], we estimate the singles rates of the experiment to be on the order of a few hundred kHz (for SHMS singles), a few hundred Hz (for HMS singles) and on the order of a few Hz for the coincidence trigger rate.

p_m (MeV/c)	θ_{nq} (deg)	data-taking (hrs)	overhead (hrs)
500	70	24	2
800	49	200	2
	60	144	2
	72	160	2
$^1\text{H}(e, e'p)$ elastic		8	
target boiling		2	
BCM calibration		2	
total		540	548 hrs (23 PAC days)

Table 4: Beam time allocation.

5 Summary

In summary, this letter of intent aims to measure for the first time the angular (θ_{nq}) distributions of the FSI/PWIA cross-section ratios for the exclusive $d(e, e'p)n$ reaction at large momentum transfers ($Q^2 = 4.5 \text{ GeV}/c^2$) and very high missing momenta ($p_m \sim 800 \text{ MeV}/c$) which corresponds to a kinematic regions where the transition from the nucleonic to quark-gluon description of matter is expected.

The previous $d(e, e'p)$ commissioning experiment [12] (including the more recently completed full version) at Hall C extended the missing momentum reach up to $940 \text{ MeV}/c$ optimized for kinematics with reduced FSI at forward angles $\theta_{nq} \sim 40^\circ$. The unexpected results of that experiment showed a possible hint of the presence of the non-nucleonic components of the deuteron [13] and reinvigorated a theoretical as well as experimental interest in this simple nucleus.

The main objective of this letter is therefore to focus on extracting the FSI/PWIA angular distributions to more precisely pin down the behavior of final-state interactions at very high missing momenta while covering a wide range of neutron recoil angles to map out the angular distributions and be able to definitively rule out any possible contributions from FSI in the kinematic region corresponding to the repulsive core of the deuteron.

References

- [1] W. Boeglin and M. Sargsian, *Modern studies of the Deuteron: From the lab frame to the light front*, *International Journal of Modern Physics E* **24** (2015) 1530003, [<https://doi.org/10.1142/S0218301315300039>].
- [2] L. L. Frankfurt, W. R. Greenberg, G. A. Miller, M. M. Sargsian and M. I. Strikman, *Color transparency effects in electron deuteron interactions at intermediate Q^{**2}* , *Z. Phys. A* **352** (1995) 97–113, [[nucl-th/9501009](#)].
- [3] L. L. Frankfurt, M. M. Sargsian and M. I. Strikman, *Feynman graphs and generalized eikonal approach to high energy knock-out processes*, *Phys. Rev. C* **56** (Aug, 1997) 1124–1137.
- [4] M. M. Sargsian, *Selected Topics in High Energy Semi-Exclusive Electro-Nuclear Reactions*, *International Journal of Modern Physics E* **10** (Dec, 2001) 405–457.
- [5] C. Ciofi degli Atti and L. P. Kaptari, *Calculations of the exclusive processes $H-2(e, e\text{-prime } p)n$, $He-3(e, e\text{-prime } p)H-2$ and $He-3(e, e\text{-prime } p)(pn)$ within a generalized Glauber approach*, *Phys. Rev. C* **71** (2005) 024005, [[nucl-th/0407024](#)].
- [6] J. Laget, *The electro-disintegration of few body systems revisited*, *Physics Letters B* **609** (2005) 49 – 56.
- [7] S. Jeschonnek and J. W. Van Orden, *New calculation for $^2H(e, e'p)n$ at gev energies*, *Phys. Rev. C* **78** (Jul, 2008) 014007.
- [8] M. M. Sargsian, *Large Q^2 electrodisintegration of the deuteron in the virtual nucleon approximation*, *Phys. Rev. C* **82** (Jul, 2010) 014612.
- [9] W. P. Ford, S. Jeschonnek and J. W. Van Orden, *$^2H(e, e'p)$ observables using a Regge model parameterization of final state interactions*, *Phys. Rev. C* **87** (2013) 054006, [[1304.0647](#)].
- [10] FOR THE HALL A COLLABORATION collaboration, W. U. Boeglin, L. Coman, P. Ambrozewicz, K. Aniol, J. Arrington, G. Batigne et al., *Probing the high momentum component of the deuteron at high Q^2* , *Phys. Rev. Lett.* **107** (Dec, 2011) 262501.
- [11] CLAS COLLABORATION collaboration, K. S. Egiyan, G. Asryan, N. Gevorgyan, K. A. Griffioen, J. M. Laget, S. E. Kuhn et al., *Experimental Study of Exclusive $^2H(e, e'p)n$ Reaction Mechanisms at High Q^2* , *Phys. Rev. Lett.* **98** (Jun, 2007) 262502.
- [12] HALL C COLLABORATION collaboration, C. Yero, D. Abrams, Z. Ahmed, A. Ahmidouch, B. Aljawineh, S. Alsalmi et al., *Probing the deuteron at very large internal momenta*, *Phys. Rev. Lett.* **125** (Dec, 2020) 262501.
- [13] M. M. Sargsian and F. Vera, *New structure in the deuteron*, *Phys. Rev. Lett.* **130** (Mar, 2023) 112502.

- [14] M. M. Sargsian, T. V. Abrahamyan, M. I. Strikman and L. L. Frankfurt, *Exclusive electrodisintegration of ${}^3\text{He}$ at high Q^2 . ii. decay function formalism*, *Phys. Rev. C* **71** (Apr, 2005) 044615.
- [15] T. D. Forest, *Off-shell electron-nucleon cross sections: The impulse approximation*, *Nuclear Physics A* **392** (1983) 232–248.
- [16] W. U. Boeglin. Private communication, October, 2019.
- [17] C. Yero, *Cross section measurements of deuteron electro-disintegration at very high recoil momenta and large 4-momentum transfers (q^2)*, 2020.